

PEG-detachable lipid-polymer hybrid nanoparticle for delivery of chemotherapy drugs to cancer cells

Jiang-bo Du*, Yan-feng Song*, Wei-liang Ye, Ying Cheng, Han Cui, Dao-zhou Liu, Miao Liu, Bang-le Zhang and Si-yuan Zhou

The experiment aimed to increase the drug-delivery efficiency of poly-lactic-co-glycolic acid (PLGA) nanoparticles. Lipid-polymer hybrid nanoparticles (LPNs-1) were prepared using PLGA as a hydrophobic core and FA-PEG-hyd-DSPE as an amphiphilic shell. Uniform and spherical nanoparticles with an average size of 185 nm were obtained using the emulsification solvent evaporation method. The results indicated that LPNs-1 showed higher drug loading compared with naked PLGA nanoparticles (NNPs). Drug release from LPNs-1 was faster in an acidic environment than in a neutral environment. LPNs-1 showed higher cytotoxicity on KB cells, A549 cells, MDA-MB-231 cells, and MDA-MB-231/ADR cells compared with free doxorubicin (DOX) and NNPs. The results also showed that, compared with free DOX and NNPs, LPNs-1 delivered more DOX to the nuclear of KB cells and MDA-MB-231/ADR cells. LPNs-1 induced apoptosis in KB cells and MDA-MB-231/ADR cells in a dose-dependent manner. The above data indicated that DOX-loaded LPNs-1 could kill not only normal tumor cells but also drug-resistant

tumor cells. These results indicated that modification of PLGA nanoparticles with FA-PEG-hyd-DSPE could considerably increase the drug-delivery efficiency and LPNs-1 had potential in the delivery of chemotherapeutic agents in the treatment of cancer. *Anti-Cancer Drugs* 25:751-766 © 2014 Wolters Kluwer Health | Lippincott Williams & Wilkins.

Anti-Cancer Drugs 2014, 25:751-766

Keywords: doxorubicin, folic acid, lipid-polymer hybrid nanoparticles, multidrug resistance

Department of Pharmaceutics, School of Pharmacy, Fourth Military Medical University, Xi'an, China

Correspondence to Si-yuan Zhou, PhD, Department of Pharmaceutics, School of Pharmacy, Fourth Military Medical University, Changle West Road 17, Shaanxi province, Xi'an 710032, China

Tel: +86 29 84776783; fax: +86 29 84779212; e-mail: zhousy@fmmu.edu.cn

*Jiang-bo Du and Yan-feng Song contributed equally to the writing of this article.

Received 2 October 2013 Revised form accepted 24 January 2014

Introduction

Polymeric nanoparticles are used widely in drug-delivery systems as they have high structural integrity, stability during storage, and controlled-release property. Besides, they can be prepared easily and functionalized into an active targeted drug-delivery system. These characteristics make them highly attractive as chemotherapeutic drug-delivery carriers [1,2]. Polymeric nanoparticles can be prepared from both natural polymers (such as chitosan) and synthetic biodegradable and biocompatible polymers (such as poly-lactic-co-glycolic acid, PLGA). PLGA nanoparticles were used as an effective nanocarrier for the encapsulation of various anticancer agents such as paclitaxel [3], 9-nitrocamptothecin [4], and cisplatin [5], and also for the encapsulation of haloperidol and estradiol [6].

However, systematic administration of the bare polymeric nanoparticles cannot be performed because they are not stable in blood circulation and can be uptaken rapidly by the reticuloendothelial system [7-10]. Macrophage cells such as the Kupffer cells in the liver play a major role in the clearance mechanism. These macrophages cannot identify the nanoparticles directly; however, they can recognize the specific opsonin adsorbed on the surface of the nanoparticles [11]. To reduce the uptake of nanoparticles by reticuloendothelial system, various lipids

conjugated with polyethylene glycol (PEG) have been grafted onto the polymeric nanoparticles to form lipid-polymer hybrid nanoparticles (LPNs) [12-17]. PEG causes a steric hindrance against the opsonin adsorption because of its hydrophilicity and brush structure on the surface of nanoparticle. As a result, PEGylated polymeric nanoparticles have shown the following characteristics: (a) prolonged in-vivo blood circulation time, (b) increased aqueous solubility and stability, (c) reduced aggregation, and (d) attenuated immunogenicity [18-22].

As an effective drug-delivery system, nanoparticles should disassemble and release drug in an efficient manner after it is localized in pathological tissues. The PEG coating, however, reduces the interactions between lipid-based nanoparticles and biological membrane, which result in delay of drug release and decrease in therapeutic efficacy [23,24]. Moreover, contact of PEGylated nanoparticles with immune cells for a long duration of time can induce the generation of a PEG-specific antibody, which significantly decreases the half-life of the subsequent doses of PEGylated nanoparticles [25,26]. This can help to explain why some PEGylated nanoparticles have shown accelerated blood clearance phenomena (ABC phenomena). Therefore, de-PEGylation is needed to enhance the drug release at the target site and the clearance of the PEGylated nanoparticles

from the circulation. A balance between PEGylation and de-PEGylation should be maintained to produce a useful and safe nanoparticle formulation [27–30].

In principle, the PEG shedding approaches are categorized as diffusible PEG conjugates and connection with a degradable linker [30]. Among these, the promising approach to shed PEG is using a linker with a predetermined cleavage point between the PEG chain and the lipid moiety. Because the nanoparticles enter cells through the endocytosis pathway and usually localize in endolysosomes where pH decreases to 5.5–6.0 in endosomes and 4.5–5.0 in lysosomes, and a redox potential exists between the extracellular space and the endosomal environment because of the rich glutathione inside the endosome [31,32] thus, chemical stimuli, such as low pH or reducing agents, have been exploited to break the linker [33–36]. Enzymatic stimuli, such as proteases, have also been explored to induce the cleavage of PEG [37].

In this experiment, we have synthesized a pH-sensitive amphiphilic block copolymer: folic acid-poly(ethyleneglycol)-2-distearoyl-*sn*-glycero-3-phosphoethanolamine (FA-PEG-hyd-DSPE), in which DSPE was connected to PEG by a hydrazone bond and FA was a targeting moiety. FA-PEG-hyd-DSPE was used to decorate PLGA nanoparticles to form LPNs with a core-shell structure. It is anticipated that these pH-sensitive LPNs can increase drug loading, shed PEG in acidic organelles in tumor cells, and release the chemotherapy drug with high efficiency.

Materials and methods

Materials

PLGA (lactic/glycolic acid molar ratio 75/25 and average molecular weight 40–75 kDa) was obtained from EVONIK Industries (Essen, Germany). Polyvinyl alcohol (molecular weight: 20 000–30 000) was purchased from Shanghai Sangon Biological Engineering Technology & Services Co. Ltd (Shanghai, China). 1,2-Distearoyl-*sn*-glycero-3-phosphoethanolamine (DSPE) was purchased from J&K Chemical (Beijing, China). Folic acid (FA), *N*-hydroxysuccinimide (NHS), dicyclohexylcarbodiimide (DCC), trifluoroacetic acid, and 3-(4,5-dimethylthiazol-2-yl)-2,5-diphenyltetrazolium bromide (MTT) were purchased from Sigma-Aldrich Company (St Louis, Missouri, USA). α -Carboxyl- ω -amino poly (ethylene glycol) (HOOC-PEG-NH₂, average molecular weight 4000) was obtained from Shanghai Yare Biotech Inc. (Shanghai, China). Doxorubicin (DOX) was purchased from Hisun Pharmaceutical Co. (Zhejiang, China). The human squamous carcinoma cell (KB cell, overexpressing folate receptor), human breast cancer cell (MDA-MB-231 cell), and the folate receptor deficient human lung adenocarcinoma epithelial cell (A549 cell) were obtained from the Institute of Biochemistry and Cell Biology, Chinese Academy of Science (Shanghai, China). The DOX-resistant cell, MDA-MB-231/ADR, was prepared in our laboratory.

Methods

Preparation of FA-PEG-hyd-DSPE

The synthesis scheme for FA-PEG-hyd-DSPE is shown in Fig. 1.

Synthesis of FA-PEG-COOH: FA (221 mg), DCC (206 mg), and NHS (115 mg) were dissolved in 4 ml dimethylsulfoxide (DMSO) and stirred at room temperature for 5 h. The stirred solution was added dropwise into an NH₂-PEG-COOH containing (100 mg) DMSO solution and stirred at room temperature overnight. Then, the mixture was filtered to remove *N,N*-dicyclohexylurea. The filtrate was diluted with 10-fold volume of water and dialyzed (molecular weight cut-off: 1000) in water for 2 days before it was collected by freeze-drying. The product was dissolved in water and the solution was further purified by Sephadex G-25. The target component was lyophilized to produce a yellow solid powder [38–40].

Synthesis of FA-PEG-NH-NH-BOC: FA-PEG-COOH (100 mg), DCC (8.2 mg), and DMAP (0.2 mg) were dissolved in 2 ml DMSO and reacted for 5 h. Then, NH₂-NH-BOC (6 mg) was added to the reaction solution. After stirring at room temperature overnight, the mixture was filtered to remove *N,N*-dicyclohexylurea. The filtrate was dialyzed in water for 2 days and then collected by freeze-drying.

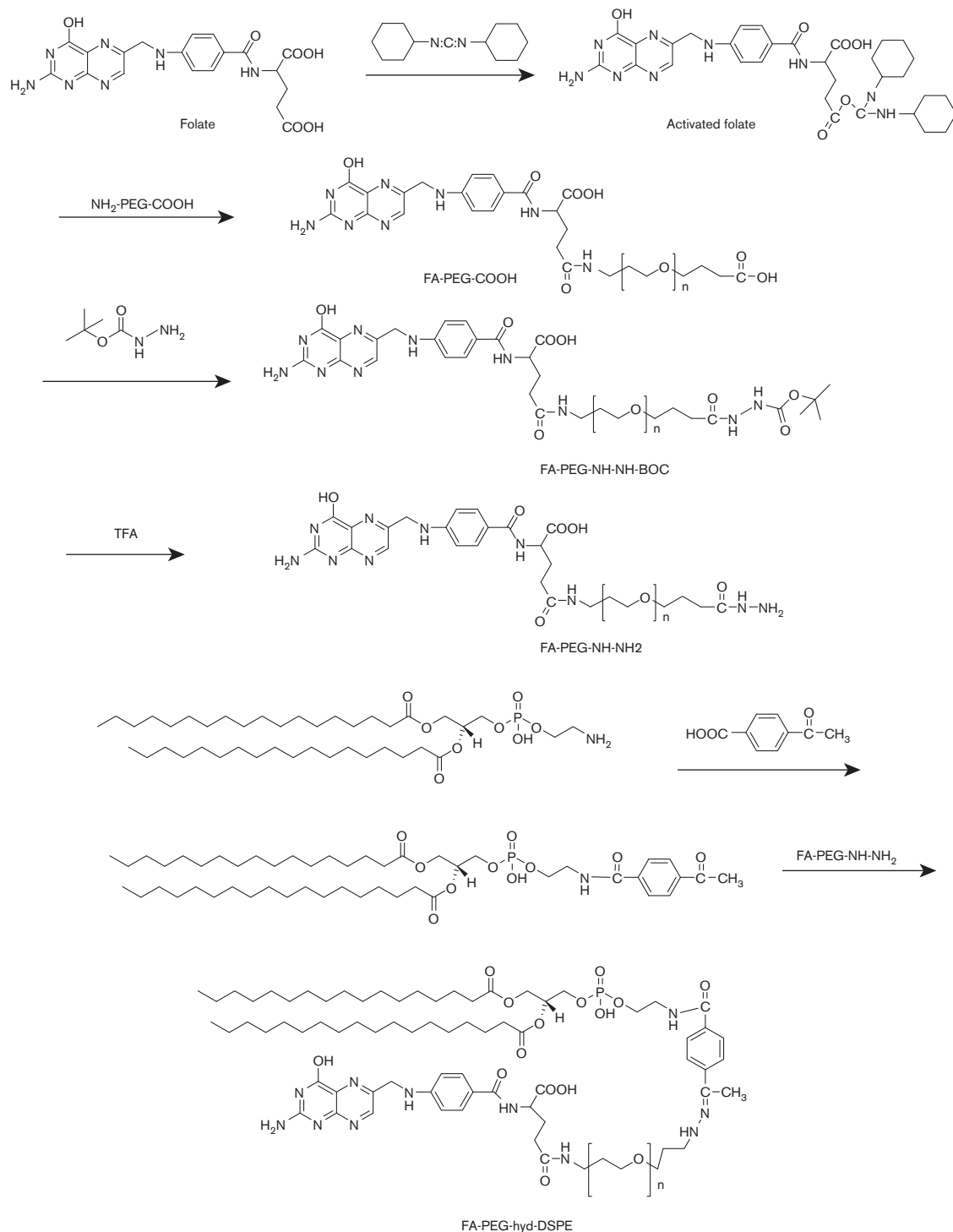
Synthesis of FA-PEG-NH-NH₂ FA-NH-NH-BOC (50 mg) was dissolved in dichloromethane and 2 ml trifluoroacetic acid was added. The mixture was reacted at room temperature for 2 h. The solvent was removed using a vacuum rotary evaporator. The residue was dialyzed and purified by Sephadex G-25 as described above.

Synthesis of DSPE-4-acetylbenzoic acid: 4-acetylbenzoic acid (30 mg), DCC (28.8 mg), and NHS (16.1 mg) were dissolved in 2 ml dichloromethane. The mixture was reacted at room temperature for 6 h before DSPE (70 mg) and triethylamine were added to the solution. After stirring at room temperature for another 6 h, the product was extracted by adding water and dichloromethane in the reaction mixture. The organic phase was dried by Na₂SO₄ and evaporated using a vacuum rotary evaporator. The residue was purified by silica gel chromatography.

Synthesis of FA-PEG-hyd-DSPE FA-PEG-NH-NH₂ (50 mg) and DSPE-acetyl benzoic acid (20 mg) were dissolved in 2 ml DMSO and reacted in the presence of trifluoroacetic acid at room temperature for 24 h. The reaction mixture was diluted with 10-fold volume of water. The solution was dialyzed and further purified by Sephadex G-25 as described above.

NH₂-PEG-hyd-DSPE NH₂-PEG-hyd-DSPE was synthesized using the same methods as FA-PEG-hyd-DSPE using NH₂-PEG-NH-NH₂ as a substrate. FA-PEG-hyd-DSPE was used as a control.

Fig. 1



Synthetic scheme of the FA-PEG-hyd-DSPE conjugate. FA-PEG-hyd-DSPE, folic acid-poly(ethyleneglycol)-2-distearoyl-*sn*-glycero-3-phosphoethanolamine.

Preparation of LPNs

The lipid-polymer hybrid PLGA nanoparticles (LPNs-1) and naked PLGA nanoparticles without FA-PEG-hyd-DSPE (NNPs) were prepared using the previously

reported method [41]. In brief, 16.0 mg PLGA and 6.0 mg FA-PEG-hyd-DSPE were dissolved in 8 ml methylene dichloride, 15 ml of 3.0% polyvinyl alcohol aqueous solution containing 3.0 mg DOX was added,

and the resulting mixture solution was sonicated in a 25 ml round-bottom flask for 30 s using a probe sonication power of 400 W in an ice bath. After stirring at room temperature for 4 h, the LPNs-1 were collected by centrifugation at 8000g (10 min) and the precipitate was washed three times by deionized water. LPNs-2 was prepared using the same methods as LPNs-1 using NH₂-PEG-hyd-DSPE as an amphiphilic shell.

Size and morphology of LPNs and NNPs

The particle size, polydispersity index, and ζ potential of LPNs and NNPs were determined at 25°C by dynamic light scattering using a Beckman Coulter Particle Analyzer (Fullerton, California, USA). Three different samples were prepared, measured, and the data were averaged. The morphology of nanoparticles was observed using transmission electron microscopy (JEOL-100CXII; JEOL, Tokyo, Japan). A drop of the sample was deposited onto a carbon-coated copper grid to create a thin film. Before the film was dried, it was counterstained with 2% phosphotungstic acid by adding a drop of the staining solution to the film. The excess solution was drained by filter paper. The grid was allowed to dry at room temperature and the sample was then determined under transmission electron microscopy.

Surface chemistry of LPNs and NNPs

The surface compositions of the DOX-loaded NNPs, DOX-free LPNs-1, and DOX-loaded LPNs-1 were investigated using an X-ray photoelectric spectrometer (XPS; RATOS AXIS His system, Shimadzu, Japan). The binding energy spectrum was analyzed from 0 to 1100 eV in a fixed transmission mode with a passing energy of 80 eV [42].

In-vitro drug-release study

Ten milligram of freshly prepared DOX-loaded LPNs or DOX-loaded NNPs was dispersed in 10 ml PBS and incubated in a water bath shaker at 37°C. At appropriate intervals, 0.2 ml supernatant was withdrawn after centrifugation at 8000g and the same volume of fresh medium was supplemented. The DOX released was quantified by fluorescence spectroscopy (970 CRT Spectrofluorophotometer; Shanghai Precision and Scientific Instrument Co. Ltd, Shanghai, China).

Cell culture conditions

KB cells were maintained in a folate-free RPMI 1640 medium. MDA-MB-231 cells, MDA-MB-231/ADR cells, and A549 cells were maintained in an RPMI 1640 medium. The cells were supplemented with 100 U/ml penicillin, 100 U/ml streptomycin, and 10% fetal bovine serum. The cells were cultured as a monolayer in a humidified atmosphere containing 5% CO₂ at 37°C.

Cytotoxicity assay

To evaluate the cytotoxicity of the free DOX and DOX-loaded LPNs or DOX-loaded NNPs, KB cells, MDA-MB-231 cells, MDA-MB-231/ADR cells, and A549 cells were used as in-vitro models. Cells were seeded in 96-well plates (10 000 cells/per well) and incubated for 12 h. Then, the cells were exposed to different concentrations of free DOX or DOX-loaded nanoparticles. Forty-eight hours after drug treatment, 20 μ l of the MTT solution (5 mg/ml) was added and incubated for 4 h at 37°C. The medium was replaced with 150 μ l of DMSO. The absorbance was measured at 490 nm using a Bio-Rad Microplate Reader (Bio-Rad Laboratories, Richmond, California, USA). The cytotoxicity of DOX or DOX-loaded nanoparticles was shown as a cell viability percentage against the respective control [43].

Evaluation of cellular uptake of LPNs-1 and NNPs

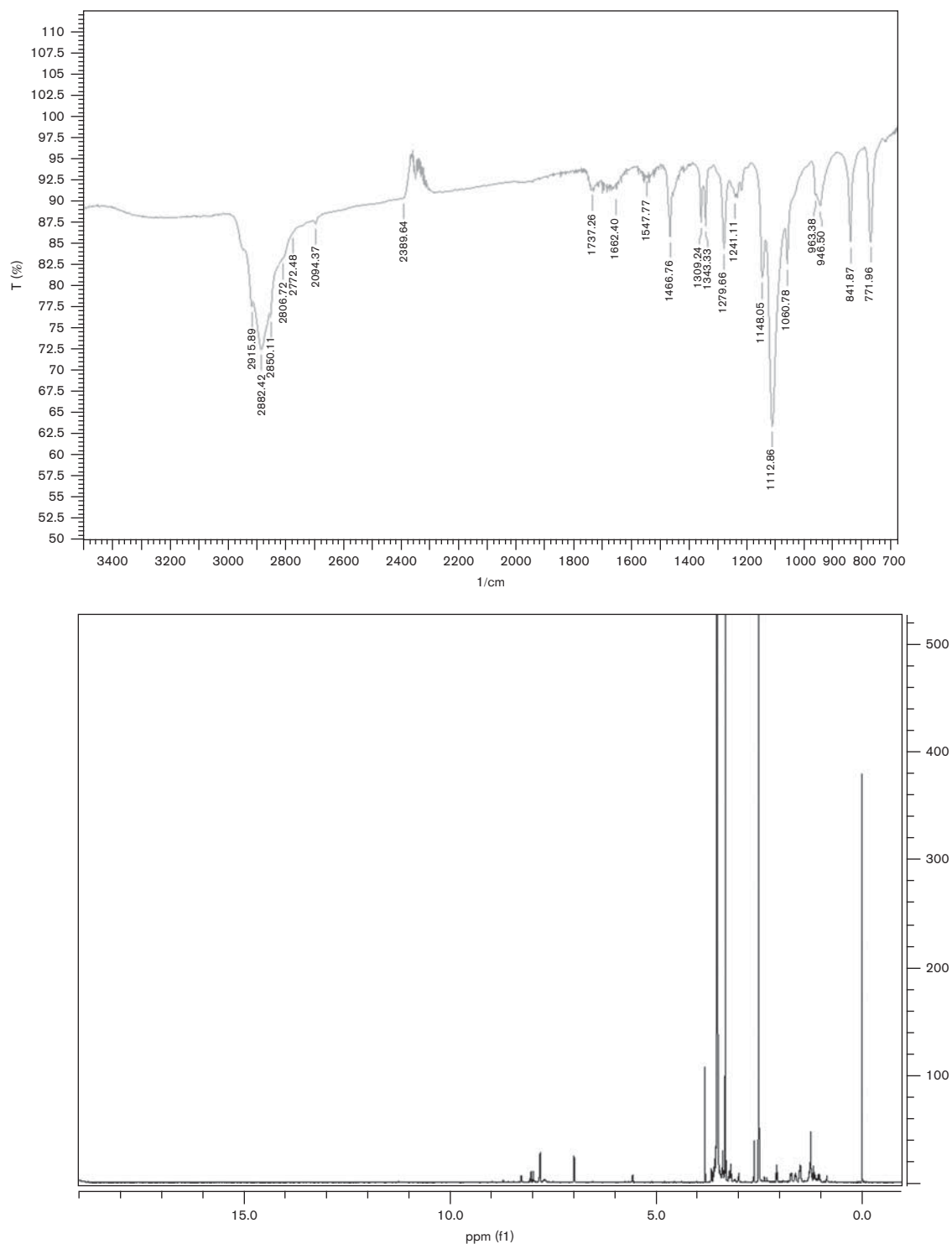
DOX shows red fluorescence, which can be used directly to investigate its cellular uptake. Cells were seeded into coverglass-containing 24-well plates at a density of 100 000 cells/well and incubated at 37°C for 12 h. DOX or DOX-loaded LPNs-1 (10 μ g/ml equivalent DOX) was added and incubated for 4 h at 37°C. The cells were then washed five times with PBS and treated with 4',6-diamidino-2-phenylindole (10 μ g/ml) for 15 min for nucleus staining. Then, the cells were washed with PBS three times and fixed with 1.5% formaldehyde. Cover slips were placed onto glass microscope slides and DOX uptake was analyzed using confocal laser scanning microscopy (Leica, Wetzlar, Germany).

Cellular uptake of DOX or DOX-loaded LPNs-1 in KB cells and MDA-MB-231/ADR cells was also determined semi-quantitatively using flow cytometry (Coulter XL, Beckman; Beckman-Coulter, Hialeah, Florida, USA). Briefly, KB cells (or MDA-MB-231/ADR cells) were seeded into 24-well plates at a cell density of 1×10^5 cells/ml. After 24 h, the medium was removed and fresh medium containing 10 μ g/ml free DOX or DOX-loaded LPNs-1 was added (200 μ l each well) and incubated with the cells at 37°C for 30 min or 3 h. The cells were collected in PBS and centrifuged for 2 min at 1000g to remove the supernatant. Finally, the cells were resuspended in 0.2 ml PBS and analyzed by flow cytometry.

Apoptosis analysis

MDA-MB-231/ADR cells and KB cells were seeded into six-well plates at a cell density of 5×10^6 cells/ml in RPMI 1640 medium. After 24 h, the medium was removed and fresh medium containing DOX or DOX-loaded LPNs-1 was added and incubated with the cells at 37°C for 24 h. Subsequently, the medium was removed and cells were washed three times with PBS, and then the cells were suspended in PBS and centrifuged for 2 min at 1000g to remove the supernatant, and the cells were resuspended in 0.2 ml PBS. After staining with annexin V-FITC and propidium iodide, the cells were analyzed by Becton Dickinson FACScan (excitation at 488 nm) (Becton Dickinson Corp., San Jose, California, USA).

Fig. 2



FTIR spectrum and ¹H NMR spectrum (dissolved in dimethylsulfoxide) of the FA-PEG-hyd-DSPE conjugate. FA-PEG-hyd-DSPE, folic acid-poly(ethyleneglycol)-2-distearoyl-*sn*-glycero-3-phosphoethanolamine.

Results and discussion

Characterization of the FA-PEG-hyd-DSPE conjugate

The FTIR spectrum and ¹H NMR spectrum of FA-PEG-hyd-DSPE are presented in Fig. 2. FA-PEG-hyd-DSPE

showed characteristic absorbance for PEG as the C-O-C etheric bond bending vibration at 1113/cm and absorption at 774/cm attributable to C-H bond vibration on the benzene ring. The absorption at 1662/cm was attributable

Fig. 3

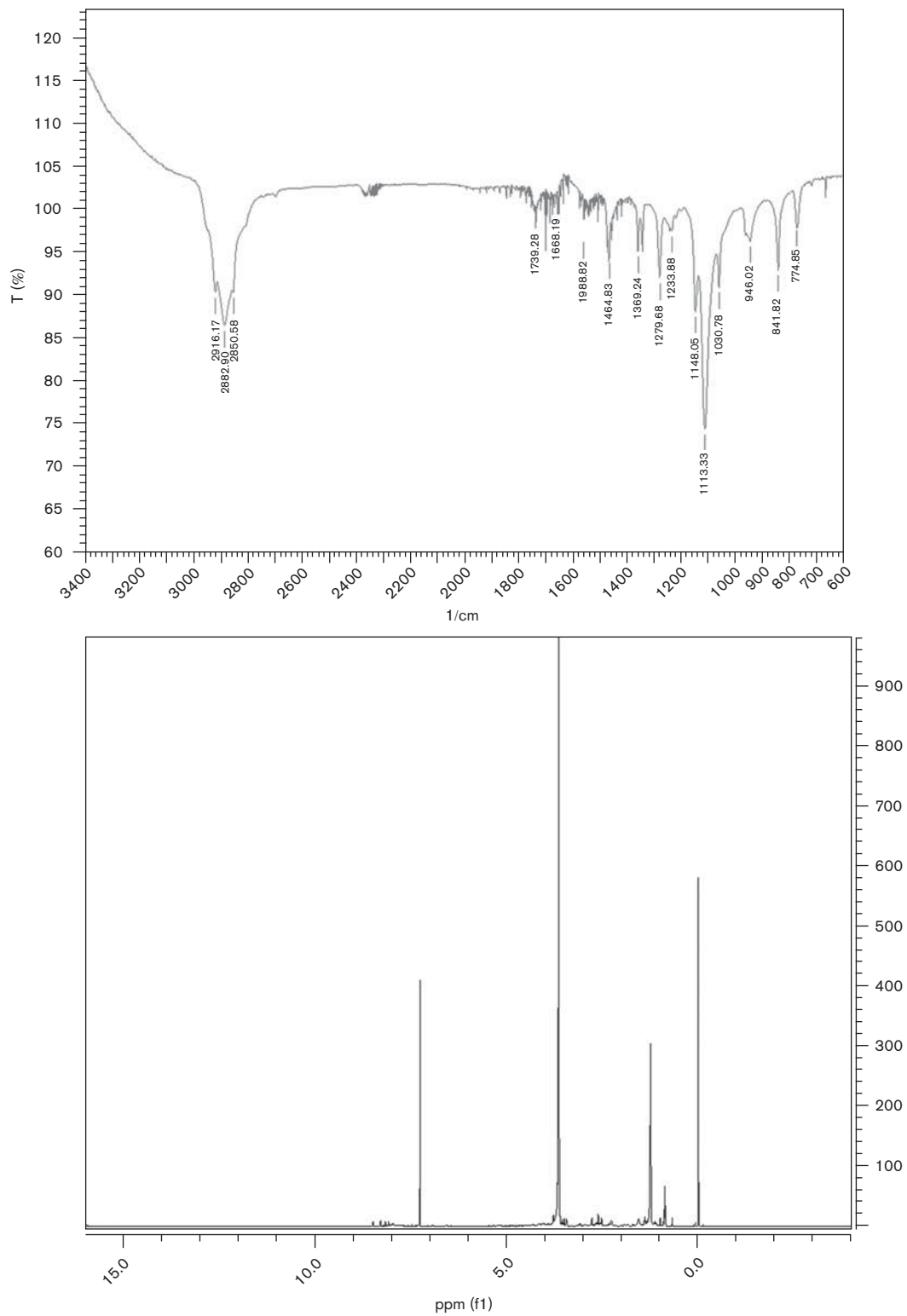
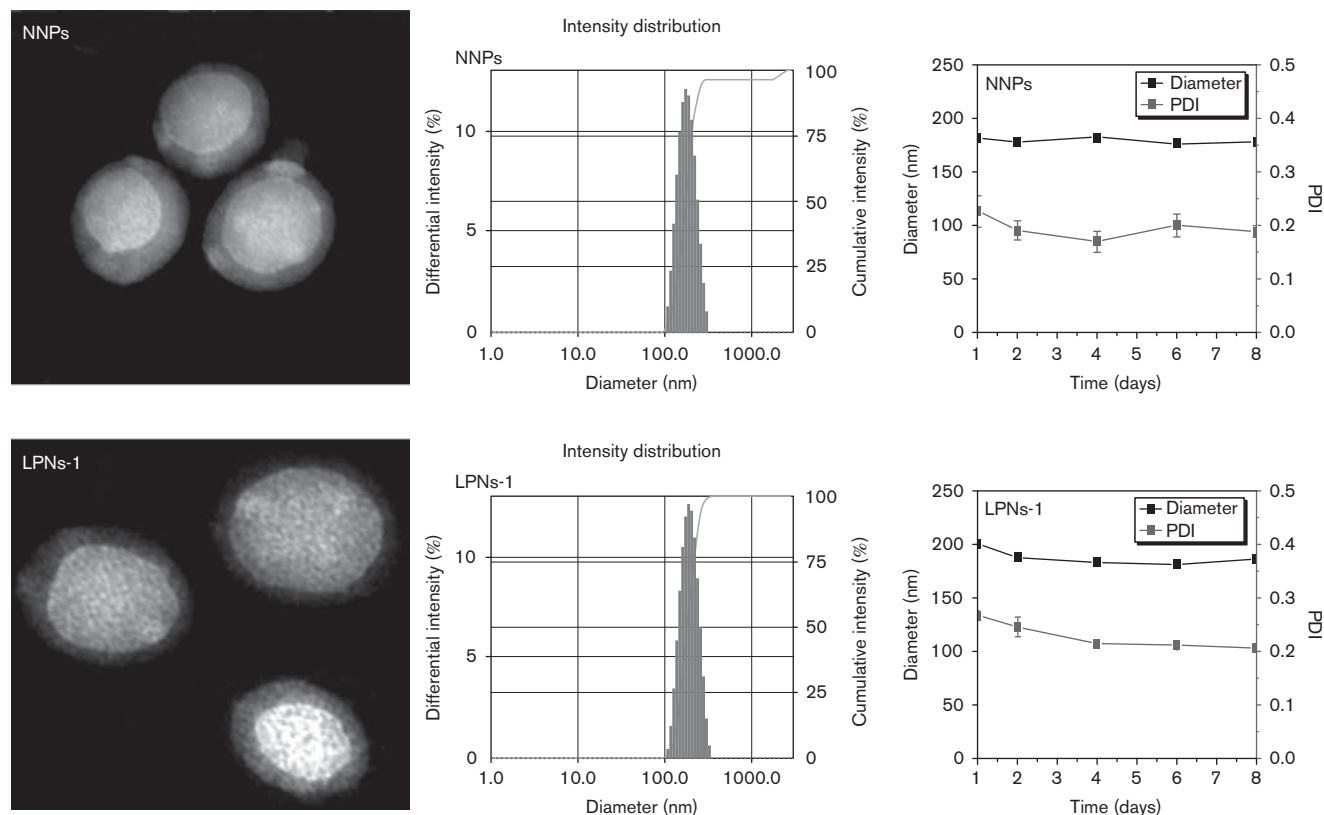
FTIR spectrum and ¹H NMR spectrum (dissolved in CHCl₃) of the PEG-hyd-DSPE conjugate.

Fig. 4



Transmission electron microscopy image, size distribution, and stability of LPNs-1 and NNPs. NNPs, naked PLGA nanoparticles; LPNs-1, FA-PEG-hyd-DSPE modified PLGA nanoparticles.

Table 1 Characteristics of nanoparticles

	Particle size (nm)	Polydispersity	ζ potential (mV)	Drug load (%)	Encapsulation efficiency (%)
LP1/PLGA=0/16 (mg/mg)	165±13	0.10±0.02	-34.5±2.7	2.2±0.3	26.7±7.3
LP1/PLGA=1/16 (mg/mg)	173±18	0.13±0.03	-29.5±1.6	3.3±0.4	48.9±8.9
LP1/PLGA=3/16 (mg/mg)	182±17	0.13±0.04	-26.3±1.2	7.8±0.7	64.3±6.2
LP1/PLGA=5/16 (mg/mg)	185±12	0.12±0.03	-25.7±1.1	9.2±2.3	76.9±8.1
LP1/PLGA=7/16 (mg/mg)	213±20	0.15±0.04	-25.8±2.7	9.3±3.0	77.7±8.5
LP2/PLGA=5/16 (mg/mg)	202±10	0.14±0.02	-16.9±1.7	6.2±1.3	56.9±6.7

LP1, FA-PEG-hyd-DSPE; LP2, PEG-hyd-DSPE; PLGA, poly-lactic-co-glycolic acid.

to stretching of the C=N bond of the hydrazone link. The presence of FA in FA-PEG-hyd-DSPE was confirmed by the appearance of signals at 7.1 and 7.8 ppm in the ^1H NMR spectrum, which corresponded with the aromatic protons of FA. Moreover, the PEG backbone was confirmed by the signal at 3.6 ppm. The FTIR spectrum and ^1H NMR spectrum of PEG-hyd-DSPE are shown in Fig. 3.

Particle characterization

When DOX-loaded nanoparticles were prepared, DOX was deprotonated by adding an excess amount of triethylamine to become hydrophobic. This is because

hydrophobic DOX is more easily entrapped in the hydrophobic core of the nanoparticles than the hydrophilic salt form DOX·HCl [42].

The morphology and stability of LPNs-1 and NNPs are shown in Fig. 4. The particle size, polydispersity index, ζ potential, drug loading, and encapsulation efficiency of LPNs and NNPs are shown in Table 1. The micrograph of LPNs-1 and NNPs showed individual nanometric particles. Both LPNs-1 and NNPs remained stable for more than 8 days in PBS.

The ζ potential of nanoparticle is a significant parameter as it plays an important role in the interaction between

cells and nanoparticles as well as suspension stability. In our experiment, the ζ potential of LPNs-1 ranged from -25.7 to -29.5 mV, whereas the ζ potential of NNPs was -34.5 mV. The ζ potential of LPNs-1 shifted toward the positive after the attachment of FA-PEG-hyd-DSPE on the surface of NNPs, which resulted from the nitrogen atoms in FA and DSPE moiety. It is established that neutral or negatively charged nanoparticles could reduce plasma protein adsorption and decrease the nonspecific cellular uptake [44,45]. However, highly positive charged nanoparticles could be removed easily from blood circulation and were not favorable for tumor targeting. Decreased nonspecific phagocytosis led to an increase in circulation time, which allowed more nanoparticles to accumulate in the tumor tissue to recognize the target cells [16]. Furthermore, the greater the ζ potential of nanoparticles, the more stable the nanoparticles suspension. This was because the charged particles repelled one another and thus overcame the natural tendency to aggregate.

The particle size, drug loading, and encapsulation efficiency of LPNs-1 increased with an increase in the content of FA-PEG-hyd-DSPE. The drug loading and encapsulation efficiency of NNPs was, respectively, 2.2 and 26.7%. When the ratio between FA-PEG-hyd-DSPE and PLGA was 6:16 (mg/mg), the particle size of LPNs-1 was 185 ± 12 nm; the drug loading and encapsulation efficiency could reach, respectively, 9.2 and 76.9%. This indicated that modification of PLGA nanoparticles with FA-PEG-hyd-DSPE not only enabled active drug delivery and long circulation but also enhanced the drug-delivery efficiency.

As is well known, particle size is a critical parameter that affects the biodistribution of nanoparticles in the body. The major pathway of extravasation for nanoparticles is through the leakage of blood vessels. The enhanced permeability and retention is an important feature of tumor tissue, which allows nanoparticles (up to 400 nm) to preferentially accumulate in tumor tissues [46,47]. It was also reported that larger polymeric nanoparticles

(> 200 nm) tended to be cleared faster in the blood, and more particles distributed in the liver, lung, and spleen. Smaller nanoparticles (10–200 nm) with less negative surface charge tended to accumulate in tumors while being cleared from the blood at a slower rate [48,49]. Besides, the degree of leakiness of the tumor blood vessel and the optimal size of the nanoparticles varied significantly among different tumor types [47]. For example, the vasculatures in human brain, pancreatic, and ovarian cancers is less leaky than those of other cancers [50,51].

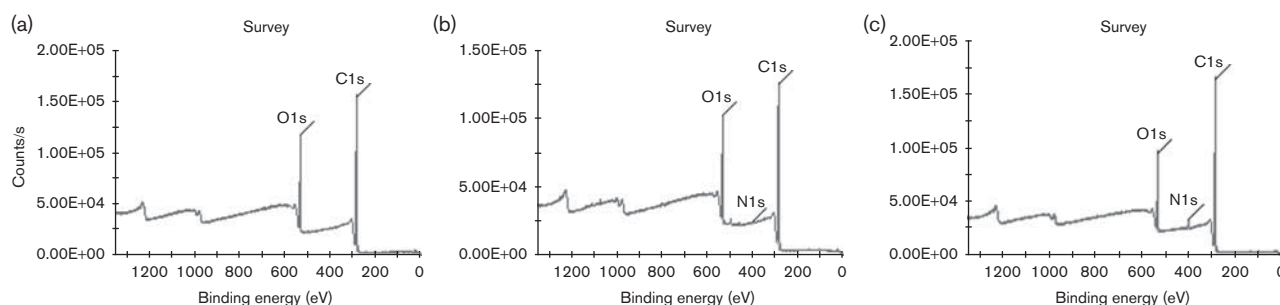
Surface chemistry

The surface chemistry of LPNs-1 and NNPs is shown in Fig. 5. The chemical composition weight percentages of nitrogen on the surface of DOX-loaded NNPs, DOX-free LPNs-1, and DOX-loaded LPNs-1 were calculated to be 0, 0.49, and 2.31%, respectively. There was one nitrogen atom in the DOX chemical structure but no N 1s signal was observed for the DOX-loaded NNPs (Fig. 5a), which indicated that DOX were well encapsulated inside the NNPs. Nevertheless, there were no nitrogen atoms in the chemical structure of PLGA and there were 11 nitrogen atoms in the FA-PEG-hyd-DSPE conjugate. There was an N 1s signal in the XPS data for DOX-free LPNs-1 (Fig. 5b), and this indicated that folate was coated on the surface of the LPNs-1 [42,52]. Thus, the DOX-loaded LPNs-1 was guided to recognize the FA high-expressed tumor cells. The N 1s percentage was found to increase to 2.31% in the DOX-loaded LPNs-1 (Fig. 5c), which indicated that some amount of DOX was encapsulated in the shell of the LPNs-1, composed of FA-PEG-hyd-DSPE. This is the main reason why LPNs-1 showed enhanced drug-loading capacity and encapsulation efficiency compared with NNPs. This discovery is consistent with the previously reported studies [53–55].

In-vitro DOX release kinetics

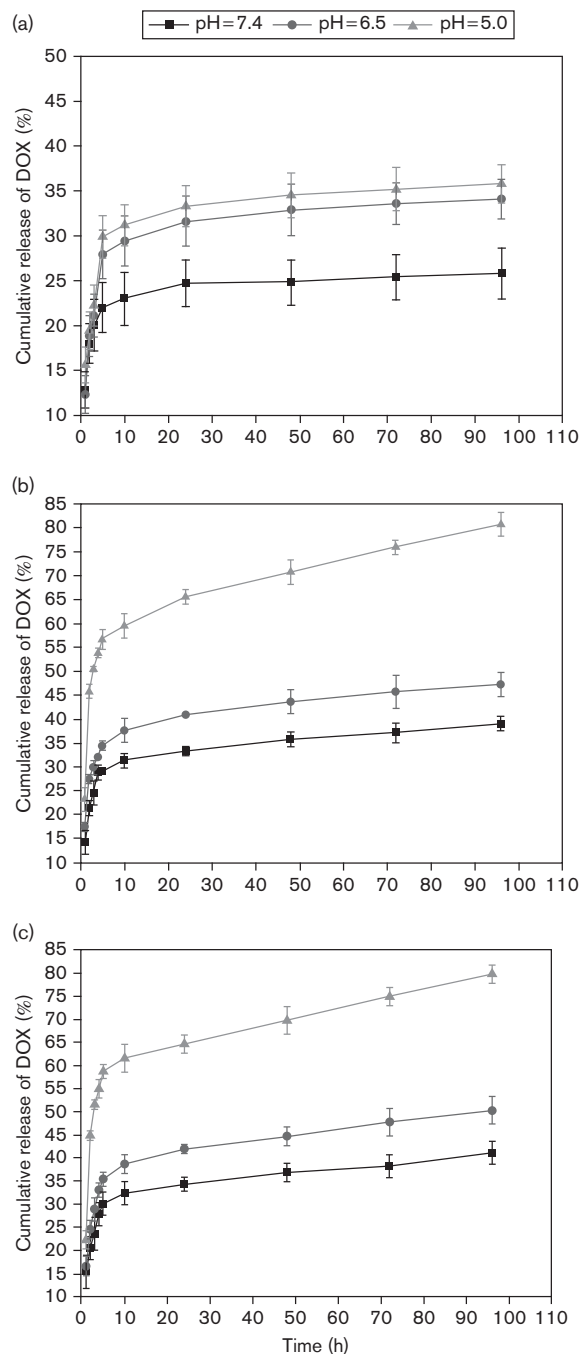
In-vitro drug-release kinetics from DOX-loaded LPNs-1, DOX-loaded LPNs-2, and DOX-loaded NNPs are shown

Fig. 5



The X-ray photoelectron spectrometer wide scan spectra of the DOX-loaded NNPs (a), DOX-free LPNs-1 (b), and DOX-loaded LPNs-1 (c). DOX, doxorubicin; LPNs-1, FA-PEG-hyd-DSPE modified PLGA nanoparticles; NNPs, naked PLGA nanoparticles.

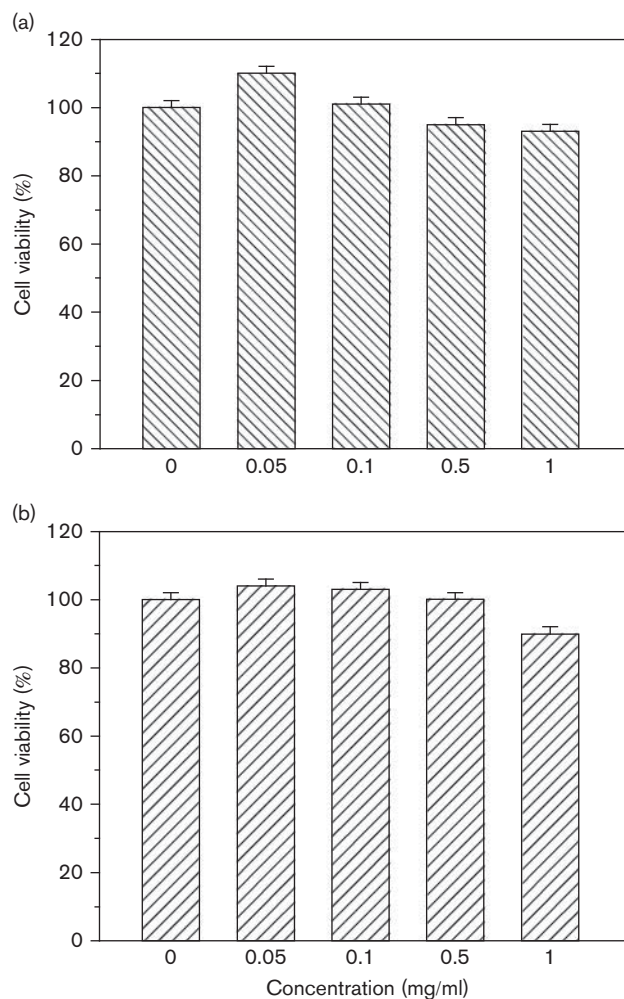
Fig. 6



Cumulative release profile of DOX from LPNs and NNPs in different pH medium *in vitro*. (a) DOX-loaded NNPs. (b) DOX-loaded LPNs-1. (c) DOX-loaded LPNs-2. DOX, doxorubicin; LPNs-1, FA-PEG-hyd-DSPE modified PLGA nanoparticles; LPNs-2, PEG-hyd-DSPE modified PLGA nanoparticles; NNPs, naked PLGA nanoparticles.

in Fig. 6. The rate and amount of DOX released from the LPNs-1 were strongly dependent on the pH of the medium. LPNs-1 showed much faster DOX release at pH

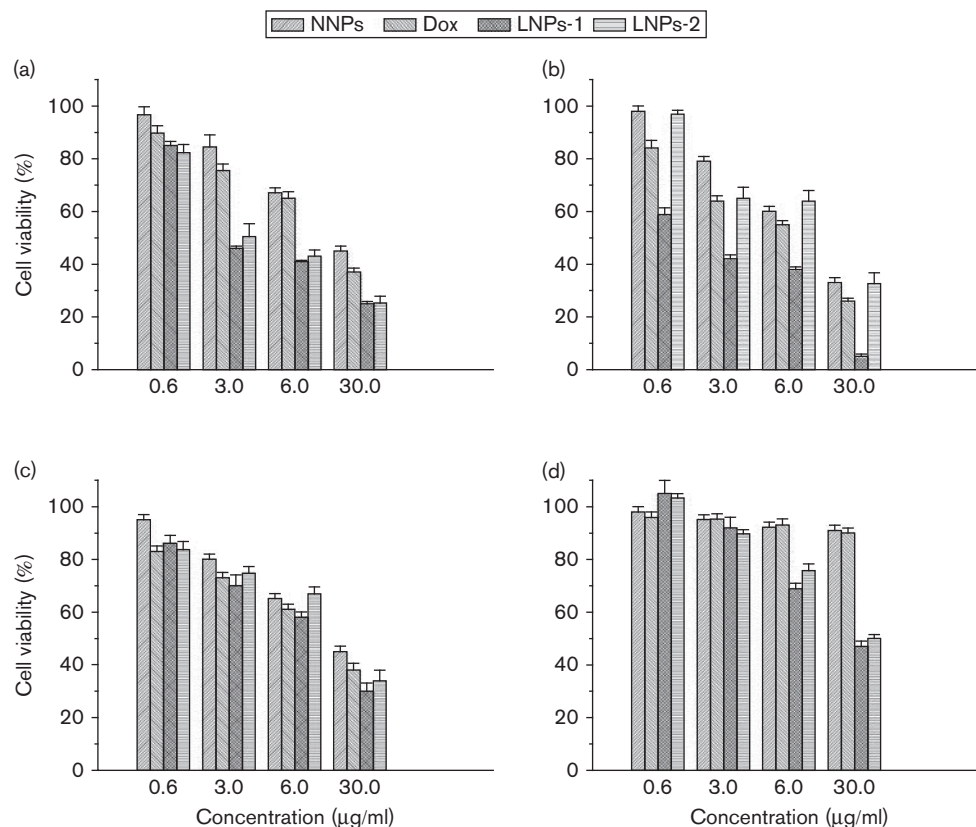
Fig. 7



The cytotoxicity of DOX-free LPNs-1 toward KB cells (a) and MDA-MB-231 cells (b). Cells were treated for 48 h. DOX, doxorubicin; LPNs-1, FA-PEG-hyd-DSPE modified PLGA nanoparticles.

5.0 than at pH 7.4. In pH 5.0 medium, LPNs-1 released 60% of the loaded DOX in 10 h. However, in pH 7.4 medium, the LPNs-1 released only 30% of the loaded DOX in 10 h. However, the rate and amount of DOX released from NNPs were much lower than those released from LPNs-1. The rate and amount of DOX released from NNPs in pH 5.0 medium were almost the same as those in pH 6.5 medium, but were higher than those in pH 7.4 medium. NNPs released 23% of the loaded DOX in 10 h in pH 7.4 medium and released about 30% of the loaded DOX in 10 h in pH 5.0 medium. The faster release of DOX from the LPNs-1 in pH 5.0 medium resulted from the hydrazone linkage breaking between the DSPE and PEG, which mimicked the drug-release behavior in endosomal/lysosomal compartments of the tumor cells. The slow DOX release rate of LPNs-1 observed in pH 7.4 medium ensured that little

Fig. 8



The cytotoxicity of DOX, DOX-loaded NNPs, DOX-loaded LPNs-1, and DOX-loaded LPNs-2 on tumor cells. DOX, doxorubicin; LPNs-1, FA-PEG-hyd-DSPE modified PLGA nanoparticles; LPNs-2, PEG-hyd-DSPE modified PLGA nanoparticles; NNPs, naked PLGA nanoparticles. (a) MDA-MB-231 cells; (b) KB cells; (c) A549 cells; (d) MDA-MB-231/ADR cells. Cells were treated for 48 h.

DOX was released from LPNs-1 during circulation in the blood.

At the same time, LPNs-1 showed a biphasic drug-release pattern characterized by an initial burst release of about 30, 37, and 60% of the total loaded DOX in the LPNs-1 in 10 h in pH 7.4, 6.4, and 5.0 medium, respectively, which was mainly because of the release of DOX entrapped in the outer lipid layer of LPNs-1. The initial burst release was followed by a slow, but sustained release. After 100 h, 80, 45, and 37% of the entrapped drug was found to be released, respectively, in pH 5.0, 6.4 and 7.4 medium. The sustained release of DOX from the LPNs-1 was attributed to diffusion-mediated release from nanoparticles and the gradual hydrolysis and corrosion of the core of LPNs-1 [56]. The faster drug release of DOX from NNPs in 6 h was mainly because of the release of DOX coated in the outer layer of NNPs. After this initial burst release, DOX was released slowly but continuously at a linear rate, indicating diffusion-mediated release from the NNPs [56].

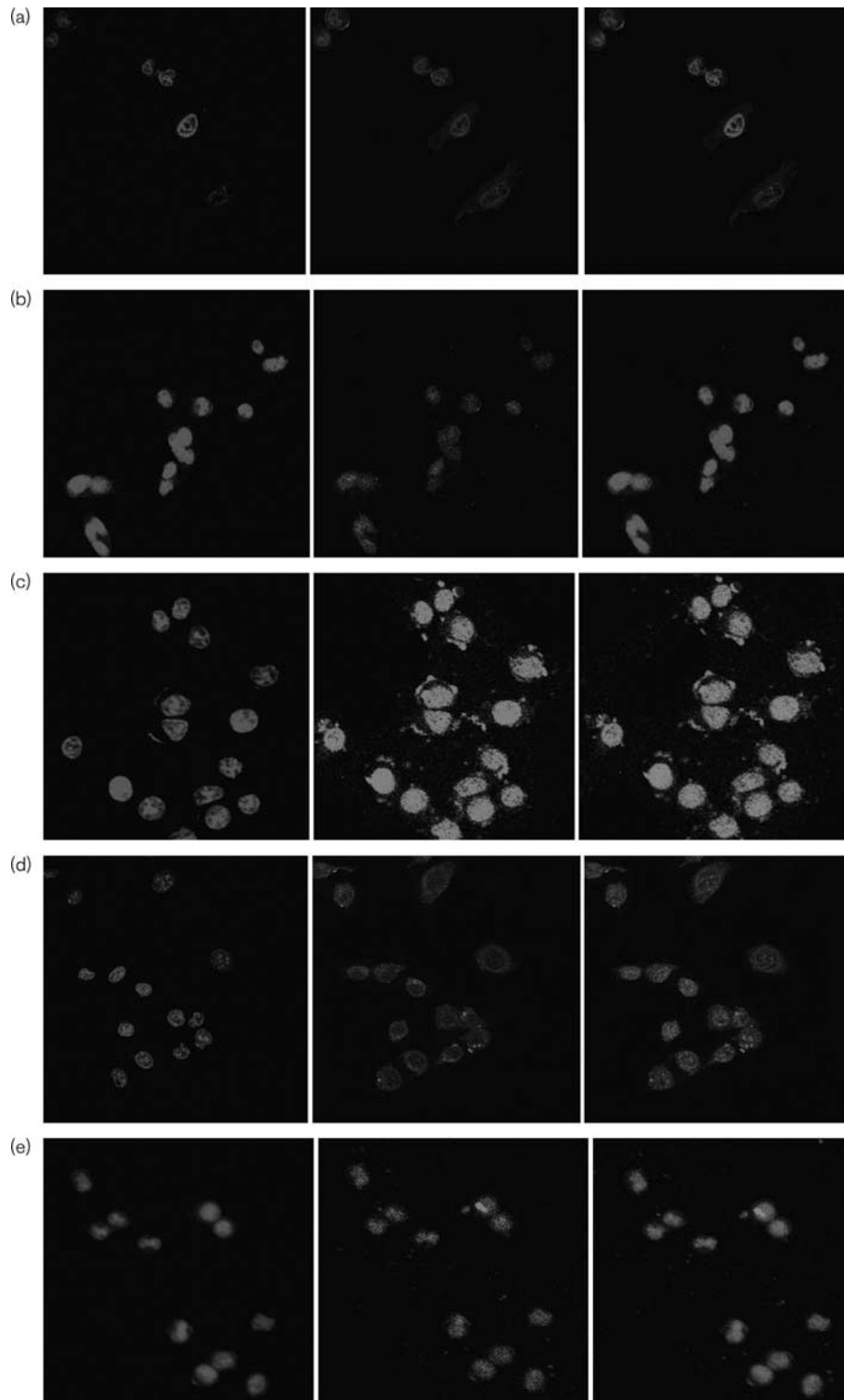
LPNs-2 showed the same drug-release characteristics as LPNs-1, which indicated that FA did not

influence the drug-release characteristics of nanoparticles *in vitro*.

Cytotoxicity of nanoparticles

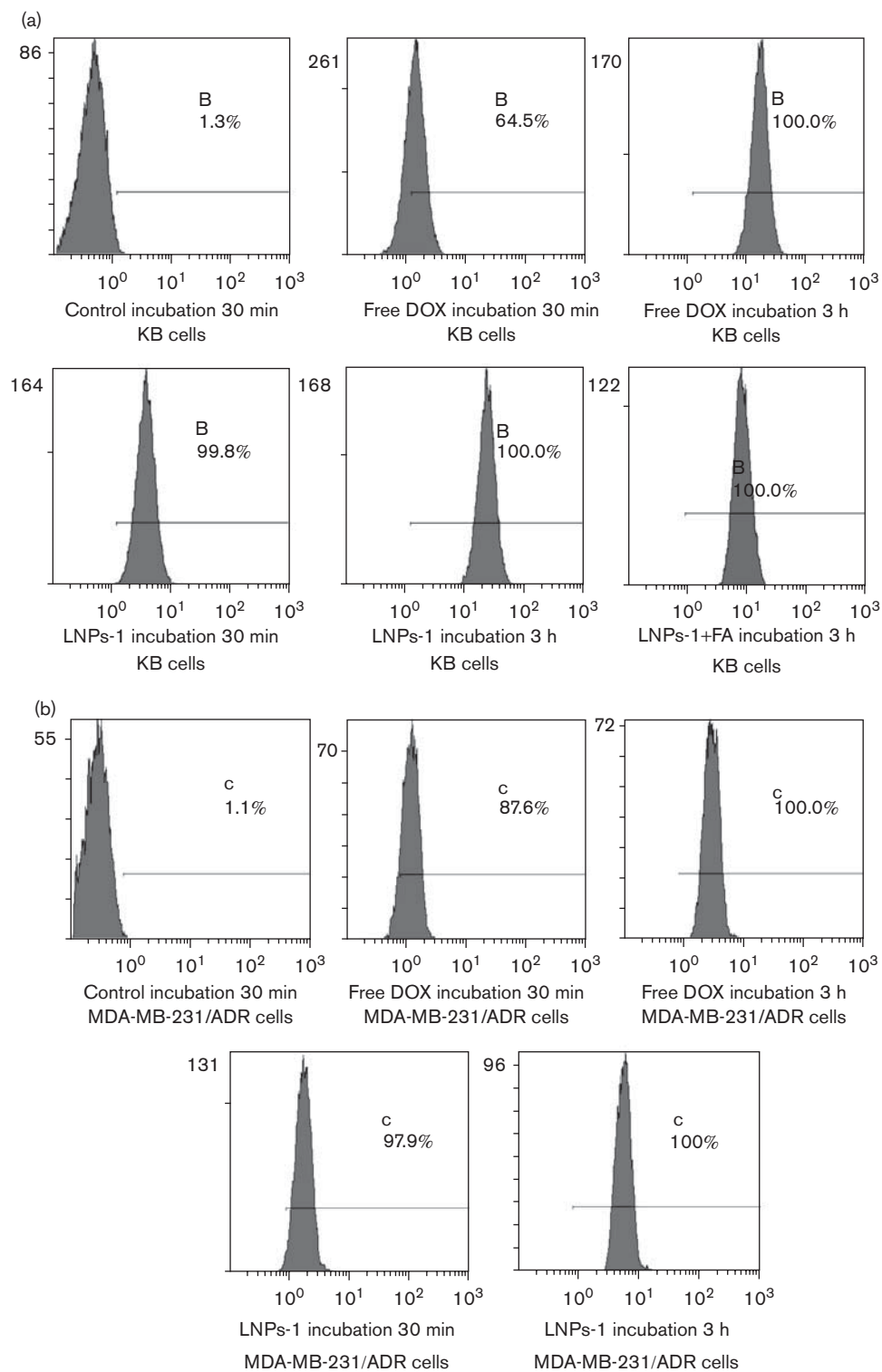
The cytotoxicity of DOX-loaded LPNs-1, DOX-loaded LPNs-2, and DOX-loaded NNPs was determined using the MTT method. Figure 7 shows the cytotoxicity of non-drug-loaded LPNs-1 on KB cells and MDA-MB-231 cells. The results indicated that non-drug-loaded LPNs-1 did not influence the cell viability, which implied that blank LPNs-1 had none of the cytotoxicity. The cytotoxicity of DOX-loaded nanoparticles is shown in Fig. 8. As the DOX concentration was increased, the viability of cancer cells was decreased. DOX-loaded LPNs-1 showed greater toxicity on KB cells, MDA-MB-231 cells, MDA-MB-231/ADR cells, and A549 cells than DOX-loaded NNPs and free DOX. Meanwhile, KB cells [folate receptor (FR) overexpression] were more sensitive to DOX-loaded LPNs-1 compared with A549 cells (FR deficient). Free DOX (3 μmol/l) killed 27, 37, and 24% of the A549 cells, KB cells, and MDA-MB-231 cells, respectively. The same dose of DOX loaded in LPNs-1 killed almost 29, 58, and 56% of the A549 cells, KB cells, and MDA-MB-231

Fig. 9



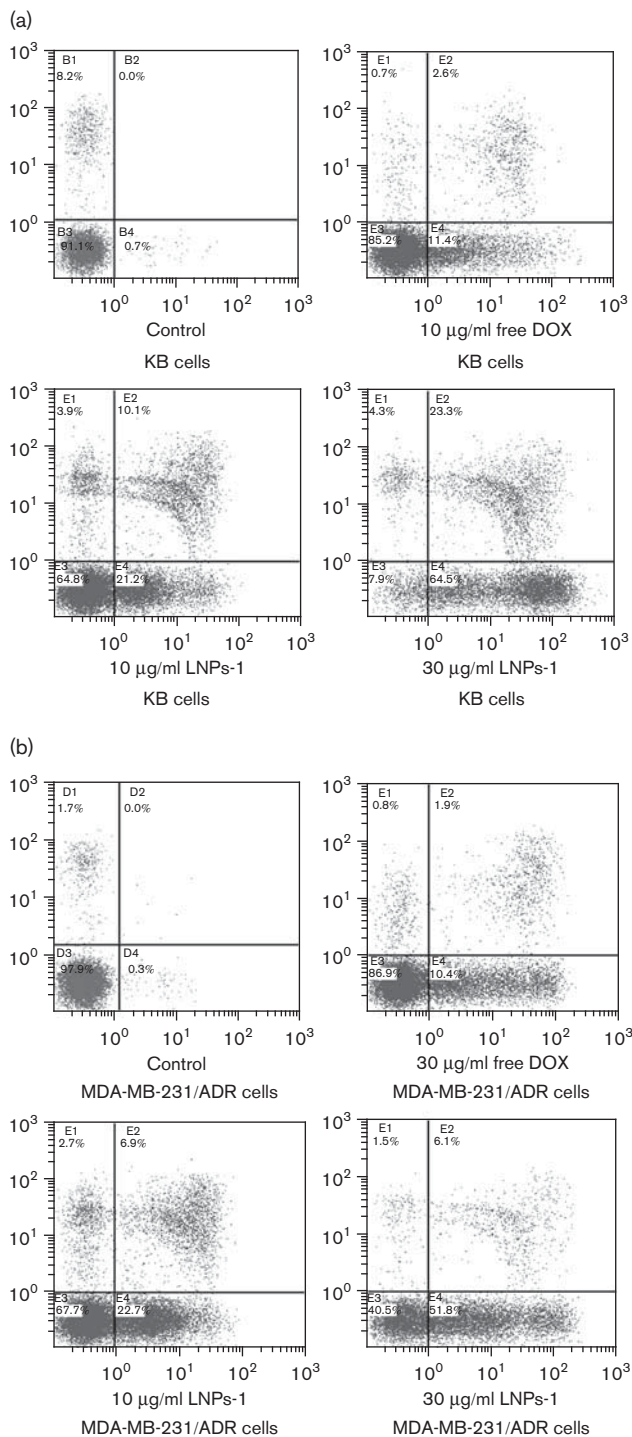
Confocal laser scanning microscopy (CLSM) images of KB cells and MDA-MB-231/ADR cells incubated with DOX, DOX-loaded NNPs, and DOX-loaded LPNs-1 at 37°C for 4 h. DOX, doxorubicin; LPNs-1, FA-PEG-hyd-DSPE modified PLGA nanoparticles; NNPs, naked PLGA nanoparticles. (a) Free DOX in KB cells. (b) DOX-loaded NNPs in KB cells. (c) DOX-loaded LPNs-1 in KB cells. (d) Free DOX in MDA-MB-231/ADR cells. (e) DOX-loaded LPNs-1 in MDA-MB-231/ADR cells. The DOX concentration was 10 µg/ml. The right column shows the left and middle columns merged, indicating the localization of DOX in the cell.

Fig. 10



Flow cytometry results of cellular uptake of free DOX and DOX-loaded LPNs-1 in 30 min and 3 h. (a) KB cells; (b) MDA-MB-231/ADR cells. The DOX concentration was 10 µg/ml. DOX, doxorubicin; LPNs-1: FA-PEG-hyd-DSPE modified PLGA nanoparticles.

Fig. 11



Apoptosis of KB cells (a) and MDA-MB-231/ADR cells (b) induced by different concentrations of DOX and DOX-loaded LPNs-1. DOX, doxorubicin; LPNs-1: FA-PEG-hyd-DSPE modified PLGA nanoparticles. KB cells and MDA-MB-231/ADR cells were treated with 10 µmol/l free DOX or 10, 30 µmol/l DOX-loaded LPNs-1 for 24 h. Cells were harvested by trypsinization and centrifugation, and then analyzed in a Becton Dickinson FACScan (excitation at 488 nm) equipped with Cell Quest software (Becton Dickinson Immunocytometry Systems, San Diego, California, USA) after staining with annexin V-FITC and propidium iodide.

cells, respectively. DOX (3 µmol/l) loaded in LPNs-2 killed almost 26, 35, and 48% of the A549 cells, KB cells, and MDA-MB-231 cells, respectively. The above data indicated that LPNs-1 enhanced the cytotoxicity of DOX, and there was no significant difference in cytotoxicity on A549 cells between LPNs-1 and LPNs-2. The high FA receptor-expressed cancer cells were more sensitive to DOX-loaded LPNs-1 compared with DOX-loaded LPNs-2. This implied that the FA in LPNs-1 played an important role in cytotoxicity on high FA receptor-expressed cancer cells.

MDA-MB-231/ADR cells were the DOX-resistant cell line. It is interesting to discover that 6 µmol/l free DOX killed 7% of the MDA-MB-231/ADR cells. However, the same dose of DOX loaded in LPNs-1 and LPNs-2 killed almost 31 and 24% of MDA-MB-231/ADR cells, respectively. This indicated that DOX-loaded LPNs could kill not only normal tumor cells but also drug-resistant tumor cells. In addition, DOX-loaded NNPs showed lower toxicity on A549 cells, KB cells, and MDA-MB-231/ADR cells compared with free DOX. The above results showed that modification of PLGA with FA-PEG-hyd-DSPE resulted in the burst release of DOX in tumor cells, and subsequently, considerably increased the cytotoxicity of DOX-loaded LPNs.

Because of its small size, nanoparticles could take advantage of the enhanced permeability and retention effect to enhance the retention time of loaded drugs in tumor tissue. A new and promising strategy was to conjugate a tumor-cell-specific ligand with nanoparticles to form an active tumor-targeting drug-delivery system, which could selectively recognize tumor cells. Subsequently, it led to a reduction in drug dose, improvement in therapeutic efficacy, and decrease in toxicity [57]. FA was one of the most commonly used tumor-cell-specific ligand as FR overexpression had been identified in a wide range of tumors such as in ovarian, endometrial, colorectal, or breast cancer [58]. Some researches showed enhanced uptake of folate-conjugated nanoparticles by cancer cells [59–61].

In-vitro cellular uptake of NPs

The main anticancer action of DOX was to inhibit topoisomerase II and cause DNA damage. Chromosomal DNA was the main action target of DOX. Thus, the subcellular distribution of DOX was evaluated by confocal laser scanning microscopy. After KB cells were treated with free DOX for 4 h, DOX was predominantly accumulated in the nucleus (Fig. 9a). When MDA-MB-231/ADR cells were treated with free DOX for 4 h, DOX was predominantly accumulated in the cytoplasm (Fig. 9d). The cellular uptake of DOX-loaded LPNs-1 in KB cells and MDA-MB-231/ADR cells is, respectively, shown in Fig. 9c and e. When KB cells and MDA-MB-231/ADR cells were incubated with DOX-loaded LPNs-1, a

large amount of DOX was distributed in the nucleus. This was expected because of the dissociation of FA-PEG-hyd-DSPE on the surface of LPNs-1 in endolysosomes, subsequently resulting in the burst release of DOX and a similar pattern of cellular distribution with free DOX. However, a small amount of DOX was distributed in the nucleus after DOX-loaded NNPs were incubated with KB cells (Fig. 9b).

The cellular uptake of free DOX and DOX-loaded LPNs-1 was further investigated semiquantitatively in KB cells and MDA-MB-231/ADR cells using flow cytometry. The results are shown in Fig. 10a and b. The cellular uptake of free DOX and DOX-loaded LPNs-1 in KB cells and MDA-MB-231/ADR cells increased in a time-dependent manner. The intracellular uptake of DOX-loaded LPNs-1 in KB cells and MDA-MB-231/ADR cells was greater than that of free DOX. When KB cells were incubated with exogenous folate and DOX-loaded LPNs-1, the uptake efficiency of DOX-loaded LPNs-1 was attenuated obviously. These results clearly indicated that cellular uptake of DOX-loaded LPNs-1 on KB cells was facilitated by receptor-mediated endocytosis.

The cytotoxic effect resulted from the release of DOX from the nanoparticles. It was reported that PLGA nanoparticles were internalized by the endocytosis process, followed by escape of endolysosomes and delivery of encapsulated agents to the cytosol [62]. The increased intranuclear delivery significantly improved the therapeutic efficacy of DOX, and a small dose of DOX entrapped in LPNs-1 could exert the same cytotoxic effects as those obtained at a high dose of free drug. One interesting discovery from our experiments was the high intranuclear distribution of DOX delivered by LPNs-1 in DOX-resistant tumor cells. The above results were consistent with the previous reports that DOX-loaded nanoparticles could overcome tumor cell multidrug resistance [63–65].

Apoptosis induced by LPNs

A number of findings supported that DOX exerted its effects by inducing apoptosis through various signaling pathways, such as the p53 and H₂O₂ pathway [66–67]. Thus, we investigated the apoptosis induced by DOX-loaded LPNs-1. KB cells and MDA-MB-231/ADR cells were incubated with different concentrations of DOX and DOX-loaded LPNs-1 for 24 h. The percentage of apoptosis was determined by flow cytometry. Representative pictures are shown in Fig. 11a and b. DOX-loaded LPNs-1 induced apoptosis in KB cells and MDA-MB-231/ADR cells in a dose-dependent manner. Compared with free DOX, DOX-loaded LPNs-1 induced much more apoptosis both in KB cells and in MDA-MB-231/ADR cells. These results were in agreement with both the MTT results and the drug-release characteristics of LPNs-1 *in vitro*.

Conclusion

The above experiment implied that modification of PLGA nanoparticles with FA-PEG-hyd-DSPE enhanced the drug loading. Compared with NNPs, LPNs-1 significantly increased the intranuclear distribution of DOX both in normal tumor cells and in DOX-resistant tumor cells. Therefore, it was concluded that modification of PLGA nanoparticles with FA-PEG-hyd-DSPE could considerably enhance the drug-delivery efficiency and it had potential in delivering chemotherapeutic agents to treat cancer.

Acknowledgements

This work was supported by the Shaanxi Science and Technology Innovation Project (2012KTCL03-18) and the Shaanxi Natural Science Foundation (2013JQ4026).

Conflicts of interest

There are no conflicts of interest.

References

- Peer D, Karp JM, Hong S, Farokhzad OC, Margalit R, Langer R. Nanocarriers as an emerging platform for cancer therapy. *Nat Nanotechnol* 2007; **2**:751–760.
- Hadinoto K, Sundaresan A, Cheow WS. Lipid-polymer hybrid nanoparticles as a new generation therapeutic delivery platform: a review. *Eur J Pharm Biopharm* 2013; **85**:427–443.
- Fonseca C, Simoes S, Gaspar R. Paclitaxel-loaded PLGA nanoparticles: preparation, physicochemical characterization and *in vitro* anti-tumoral activity. *J Control Release* 2002; **83**:273–286.
- Derakhshandeh K, Erfan M, Dadashzadeh S. Encapsulation of 9-nitrocamptothecin, a novel anticancer drug, in biodegradable nanoparticles: factorial design, characterization and release kinetics. *Eur J Pharm Biopharm* 2007; **66**:34–41.
- Avgoustakis K, Beletsi A, Panagi Z, Klepetsanis P, Karydas AG, Ithakissios DS. PLGA-mPEG nanoparticles of cisplatin: *in vitro* nanoparticle degradation, *in vitro* drug release and *in vivo* drug residence in blood properties. *J Control Release* 2002; **79**:123–135.
- Budhian A, Siegel SJ, Winey KI. Production of haloperidol-loaded PLGA nanoparticles for extended controlled drug release of haloperidol. *J Microencapsul* 2005; **22**:773–785.
- Yamamoto Y, Nagasaki Y, Kato Y, Sugiyama Y, Kataoka K. Long-circulating poly(ethylene glycol)-poly(D,L-lactide) block copolymer micelles with modulated surface charge. *J Control Release* 2001; **77**:27–38.
- Sheng Y, Yuan Y, Liu C, Tao X, Shan X, Xu F. *In vitro* macrophage uptake and *in vivo* biodistribution of PLA-PEG nanoparticles loaded with hemoglobin as blood substitutes: effect of PEG content. *J Mater Sci Mater Med* 2009; **20**:1881–1891.
- Braasch DA, Paroo Z, Constantinescu A, Ren G, Oz OK, Mason RP, et al. Biodistribution of phosphodiester and phosphorothioate siRNA. *Bioorg Med Chem Lett* 2004; **14**:1139–1143.
- Van de Water FM, Boerman OC, Wouterse AC, Peters JG, Russel FG, Masereeuw R. Intravenously administered short interfering RNA accumulates in the kidney and selectively suppresses gene function in renal proximal tubules. *Drug Metab Dispos* 2006; **34**:1393–1397.
- Owens DE 3rd, Peppas NA. Opsonization, biodistribution, and pharmacokinetics of polymeric nanoparticles. *Int J Pharm* 2006; **307**:93–102.
- Mori A, Klibanov AL, Torchilin VP, Huang L. Influence of the steric barrier activity of amphipathic poly(ethyleneglycol) and ganglioside GM1 on the circulation time of liposomes and on the target binding of immunoliposomes *in vivo*. *FEBS Lett* 1991; **284**:263–266.
- Woodle MC, Matthay KK, Newman MS, Hidayat JE, Collins LR, Redemann C, et al. Versatility in lipid compositions showing prolonged circulation with sterically stabilized liposomes. *Biochim Biophys Acta* 1992; **1105**:193–200.
- Beletsi A, Panagi Z, Avgoustakis K. Biodistribution properties of nanoparticles based on mixtures of PLGA with PLGA-PEG diblock copolymers. *Int J Pharm* 2005; **298**:233–241.

- 15 Suh J, Choy KL, Lai SK, Suk JS, Tang BC, Prabhu S, *et al.* PEGylation of nanoparticles improves their cytoplasmic transport. *Int J Nanomedicine* 2007; **2**:735–741.
- 16 Thamake SI, Raut SL, Ranjan AP, Gryczynski Z, Vishwanatha JK. Surface functionalization of PLGA nanoparticles by non-covalent insertion of a homo-bifunctional spacer for active targeting in cancer therapy. *Nanotechnology* 2011; **22**:035101.
- 17 Feng L, Mumper RJ. A critical review of lipid-based nanoparticles for taxane delivery. *Cancer Lett* 2013; **334**:157–175.
- 18 Otsuka H, Nagasaki Y, Kataoka K. PEGylated nanoparticles for biological and pharmaceutical applications. *Adv Drug Deliv Rev* 2003; **55**:403–419.
- 19 Sheng Y, Liu C, Yuan Y, Tao X, Yang F, Shan X, *et al.* Long-circulating polymeric nanoparticles bearing a combinatorial coating of PEG and water-soluble chitosan. *Biomaterials* 2009; **30**:2340–2348.
- 20 Roser M, Fischer D, Kissel T. Surface-modified biodegradable albumin nano- and microspheres. II: effect of surface charges on in vitro phagocytosis and biodistribution in rats. *Eur J Pharm Biopharm* 1998; **46**:255–263.
- 21 Vonarbourg A, Passirani C, Saulnier P, Benoit JP. Parameters influencing the stealthiness of colloidal drug delivery systems. *Biomaterials* 2006; **27**:4356–4373.
- 22 Sengupta S, Eavarone D, Capila I, Zhao G, Watson N, Kiziltepe T, *et al.* Temporal targeting of tumour cells and neovasculature with a nanoscale delivery system. *Nature* 2005; **436**:568–572.
- 23 Parr MJ, Masin D, Cullis PR, Bally MB. Accumulation of liposomal lipid and encapsulated doxorubicin in murine Lewis lung carcinoma: the lack of beneficial effects by coating liposomes with poly(ethylene glycol). *J Pharmacol Exp Ther* 1997; **280**:1319–1327.
- 24 Hong RL, Huang CJ, Tseng YL, Pang VF, Chen ST, Liu JJ, *et al.* Direct comparison of liposomal doxorubicin with or without polyethylene glycol coating in C-26 tumor-bearing mice: is surface coating with polyethylene glycol beneficial? *Clin Cancer Res* 1999; **5**:3645–3652.
- 25 Semple SC, Harasym TO, Clow KA, Ansell SM, Klimuk SK, Hope MJ. Immunogenicity and rapid blood clearance of liposomes containing polyethylene glycol-lipid conjugates and nucleic acid. *J Pharmacol Exp Ther* 2005; **312**:1020–1026.
- 26 Ishida T, Wang X, Shimizu T, Nawata K, Kiwada H. PEGylated liposomes elicit an anti-PEG IgM response in a T cell-independent manner. *J Control Release* 2007; **122**:349–355.
- 27 Judge A, McClintock K, Phelps JR, Maclachlan I. Hypersensitivity and loss of disease site targeting caused by antibody responses to PEGylated liposomes. *Mol Ther* 2006; **13**:328–337.
- 28 Tagami T, Nakamura K, Shimizu T, Ishida T, Kiwada H. Effect of siRNA in PEG-coated siRNA-lipoplex on anti-PEG IgM production. *J Control Release* 2009; **137**:234–240.
- 29 Tagami T, Nakamura K, Shimizu T, Yamazaki N, Ishida T, Kiwada H. CpG motifs in pDNA-sequences increase anti-PEG IgM production induced by PEG-coated pDNA-lipoplexes. *J Control Release* 2010; **142**:160–166.
- 30 Huang L, Liu Y. In vivo delivery of RNAi with lipid-based nanoparticles. *Annu Rev Biomed Eng* 2011; **13**:507–530.
- 31 Mandel R, Ryser HJ, Niaki B, Ghani F, Shen WC. Isolation of variants of Chinese hamster ovary cells with abnormally low levels of GSH: decreased ability to cleave endocytosed disulfide bonds. *J Cell Physiol* 1991; **149**:60–65.
- 32 Short S, Merkel BJ, Caffrey R, McCoy KL. Defective antigen processing correlates with a low level of intracellular glutathione. *Eur J Immunol* 1996; **26**:3015–3020.
- 33 Guo X, Szoka FC Jr. Steric stabilization of fusogenic liposomes by a low-pH sensitive PEG – diortho ester – lipid conjugate. *Bioconjug Chem* 2001; **12**:291–300.
- 34 Walker GF, Fella C, Pelisek J, Fahrmeir J, Boeckle S, Ogris M, *et al.* Toward synthetic viruses: endosomal pH-triggered deshielding of targeted polyplexes greatly enhances gene transfer in vitro and in vivo. *Mol Ther* 2005; **11**:418–425.
- 35 Zhang JX, Zalipsky S, Mullah N, Pechar M, Allen TM. Pharmacological attributes of dioleoylphosphatidylethanolamine/cholesterylhemisuccinate liposomes containing different types of cleavable lipopolymers. *Pharmacol Res* 2004; **49**:185–198.
- 36 Zalipsky S, Qazen M, Walker JA 2nd, Mullah N, Quinn YP, Huang SK. New detachable poly(ethylene glycol) conjugates: cysteine-cleavable lipopolymers regenerating natural phospholipid, diacyl phosphatidylethanolamine. *Bioconjug Chem* 1999; **10**:703–707.
- 37 Hatakeyama H, Akita H, Kogure K, Oishi M, Nagasaki Y, Kihira Y, *et al.* Development of a novel systemic gene delivery system for cancer therapy with a tumor-specific cleavable PEG-lipid. *Gene Ther* 2007; **14**:68–77.
- 38 Li H, Sun X, Zhao D, Zhang Z. A cell-specific poly(ethylene glycol) derivative with a wheat-like structure for efficient gene delivery. *Mol Pharm* 2012; **9**:2974–2985.
- 39 Scomparin A, Salmaso S, Bersani S, Satchi-Fainaro R, Caliceti P. Novel folated and non-folated pullulan bioconjugates for anticancer drug delivery. *Eur J Pharm Sci* 2011; **42**:547–558.
- 40 Hwa Kim S, Hoon Jeong J, Joe CO, Gwan Park T. Folate receptor mediated intracellular protein delivery using PLL-PEG-FOL conjugate. *J Control Release* 2005; **103**:625–634.
- 41 Mieszawska AJ, Gianella A, Cormode DP, Zhao Y, Meijerink A, Langer R, *et al.* Engineering of lipid-coated PLGA nanoparticles with a tunable payload of diagnostically active nanocrystals for medical imaging. *Chem Commun (Camb)* 2012; **48**:5835–5837.
- 42 Zhang Z, Huey Lee S, Feng SS. Folate-decorated poly(lactide-co-glycolide)-vitamin E TPGS nanoparticles for targeted drug delivery. *Biomaterials* 2007; **28**:1889–1899.
- 43 Misra R, Sahoo SK. Intracellular trafficking of nuclear localization signal conjugated nanoparticles for cancer therapy. *Eur J Pharm Sci* 2010; **39**:152–163.
- 44 Alexis F, Pridgen E, Molnar LK, Farokhzad OC. Factors affecting the clearance and biodistribution of polymeric nanoparticles. *Mol Pharm* 2008; **5**:505–515.
- 45 Aggarwal P, Hall JB, McLeland CB, Dobrovolskaia MA, McNeil SE. Nanoparticle interaction with plasma proteins as it relates to particle biodistribution, biocompatibility and therapeutic efficacy. *Adv Drug Deliv Rev* 2009; **61**:428–437.
- 46 Smith AM, Duan H, Mohs AM, Nie S. Bioconjugated quantum dots for in vivo molecular and cellular imaging. *Adv Drug Deliv Rev* 2008; **60**:1226–1240.
- 47 Hobbs SK, Monsky WL, Yuan F, Roberts WG, Griffith L, Torchilin VP, *et al.* Regulation of transport pathways in tumor vessels: role of tumor type and microenvironment. *Proc Natl Acad Sci U S A* 1998; **95**:4607–4612.
- 48 He C, Hu Y, Yin L, Tang C, Yin C. Effects of particle size and surface charge on cellular uptake and biodistribution of polymeric nanoparticles. *Biomaterials* 2010; **31**:3657–3666.
- 49 Attia AB, Yang C, Tan JP, Gao S, Williams DF, Hedrick JL, *et al.* The effect of kinetic stability on biodistribution and anti-tumor efficacy of drug-loaded biodegradable polymeric micelles. *Biomaterials* 2013; **34**:3132–3140.
- 50 Jain RK. Delivery of molecular medicine to solid tumors. *Science* 1996; **271**:1079–1080.
- 51 Olive KP, Jacobetz MA, Davidson CJ, Gopinathan A, McIntyre D, Honess D, *et al.* Inhibition of Hedgehog signaling enhances delivery of chemotherapy in a mouse model of pancreatic cancer. *Science* 2009; **324**:1457–1461.
- 52 Park EK, Lee SB, Lee YM. Preparation and characterization of methoxy poly(ethylene glycol)/poly(epsilon-caprolactone) amphiphilic block copolymeric nanospheres for tumor-specific folate-mediated targeting of anticancer drugs. *Biomaterials* 2005; **26**:1053–1061.
- 53 Saxena V, Naguib Y, Hussain MD. Folate receptor targeted 17-allylamino-17-demethoxygeldanamycin (17-AAG) loaded polymeric nanoparticles for breast cancer. *Colloids Surf B Biointerfaces* 2012; **94**:274–280.
- 54 Tao W, Zeng X, Liu T, Wang Z, Xiong Q, Ouyang C, *et al.* Docetaxel-loaded nanoparticles based on star-shaped mannitol-core PLGA-TPGS diblock copolymer for breast cancer therapy. *Acta Biomater* 2013; **9**:8910–8920.
- 55 Zeng X, Tao W, Mei L, Huang L, Tan C, Feng SS. Cholic acid-functionalized nanoparticles of star-shaped PLGA-vitamin E TPGS copolymer for docetaxel delivery to cervical cancer. *Biomaterials* 2013; **34**:6058–6067.
- 56 Park J, Fong PM, Lu J, Russell KS, Booth CJ, Saltzman WM, *et al.* PEGylated PLGA nanoparticles for the improved delivery of doxorubicin. *Nanomedicine* 2009; **5**:410–418.
- 57 Sudimack J, Lee RJ. Targeted drug delivery via the folate receptor. *Adv Drug Deliv Rev* 2000; **41**:147–162.
- 58 Xia W, Low PS. Folate-targeted therapies for cancer. *J Med Chem* 2010; **53**:6811–6824.
- 59 Ulbrich K, Michaelis M, Rothweiler F, Knobloch T, Sithisam P, Cinatl J, *et al.* Interaction of folate-conjugated human serum albumin (HSA) nanoparticles with tumour cells. *Int J Pharm* 2011; **406**:128–134.
- 60 Yang SJ, Lin FH, Tsai HM, Lin CF, Chin HC, Wong JM, *et al.* Alginate-folic acid-modified chitosan nanoparticles for photodynamic detection of intestinal neoplasms. *Biomaterials* 2011; **32**:2174–2182.
- 61 Martinez A, Olmo R, Iglesias I, Tejjón JM, Blanco MD. Folate-targeted nanoparticles based on albumin and albumin/alginate mixtures as controlled release systems of tamoxifen: synthesis and in vitro characterization. *Pharm Res* 2014; **31**:182–193.

- 62 Shen H, Ackerman AL, Cody V, Giodini A, Hinson ER, Cresswell P, *et al.* Enhanced and prolonged cross-presentation following endosomal escape of exogenous antigens encapsulated in biodegradable nanoparticles. *Immunology* 2006; **117**:78–88.
- 63 Lamprecht A, Benoit JP. Etoposide nanocarriers suppress glioma cell growth by intracellular drug delivery and simultaneous P-glycoprotein inhibition. *J Control Release* 2006; **112**:208–213.
- 64 Soma CE, Dubernet C, Barratt G, Nemati F, Appel M, Benita S, *et al.* Ability of doxorubicin-loaded nanoparticles to overcome multidrug resistance of tumor cells after their capture by macrophages. *Pharm Res* 1999; **16**:1710–1716.
- 65 Wong HL, Bendayan R, Rauth AM, Wu XY. Simultaneous delivery of doxorubicin and GG918 (Elacridar) by new polymer-lipid hybrid nanoparticles (PLN) for enhanced treatment of multidrug-resistant breast cancer. *J Control Release* 2006; **116**:275–284.
- 66 Wang S, Konorev EA, Kotamraju S, Joseph J, Kalivendi S, Kalyanaraman B. Doxorubicin induces apoptosis in normal and tumor cells via distinctly different mechanisms. Intermediacy of H(2)O(2)- and p53-dependent pathways. *J Biol Chem* 2004; **279**:25535–25543.
- 67 Mizutani H, Tada-Oikawa S, Hiraku Y, Kojima M, Kawanishi S. Mechanism of apoptosis induced by doxorubicin through the generation of hydrogen peroxide. *Life Sci* 2005; **76**:1439–1453.